0022-1554/95/$3.30
The Journal of Histochemistry and Cytochemistry

Vol. 43, No. 10, pp. 1005–1018, 1995
Printed in U.S.A.

Original Article

Saponin Pre-treatment in Pre-embedding Electron Microscopic In Situ Hybridization for Detection of Specific RNA Sequences in Cultured Cells: A Methodological Study[1]

MERRYN V. E. MACVILLE,[2] KARIEN C. WIESMEIJER, ROELAND W. DIRKS, JACK A. M. FRANSEN,[3] and ANTON K. RAAP

Departments of Cytochemistry & Cytometry (MVEM,KCW,RWD,AKR) and Electron Microscopy (MVEM,KCW,JAMF), University of Leiden, Leiden, The Netherlands.

Received for publication February 13, 1995 and in revised form May 16, 1995; accepted May 20, 1995 (5A3599).

We describe a method for detection of specific RNA targets in cultured cells at the electron microscopic (EM) level using pre-embedding in situ hybridization (ISH). The specimens were monitored by reflection-contrast microscopy (RCM) before processing for EM. A good balance between preservation of ultrastructure and intensity of hybridization signals was obtained by using mild aldehyde fixation followed by saponin permeabilization. Digoxigenin-labeled probes were used for detection of human elongation factor (HEF) mRNA in HeLa cells, immediate early (IE) mRNA in rat 9G cells, and 28S rRNA in both cell lines. The hybrids were detected immunocytochemically by the peroxidase/diaminobenzidine (DAB) method or by ultra-small gold with silver enhancement. Comparison of these methods favored the peroxidase/DAB system. The accessibility of RNA in the different cell compartments was dependent on the extent of cross-linking during primary fixation even after permeabilization with saponin. By using the most optimal ISH protocol and the peroxidase/DAB system, we detected 28S rRNA over all ribosomes in the cytoplasm but not in the nucleoli, and IE mRNA in a large spot with many smaller spots around it in the nucleoplasm as well as in speckles over the cytoplasm. The sensitivity of the method is such that HEF housekeeping gene transcripts were detected in the cytoplasm. (*J Histochem Cytochem 43:1005–1018, 1995*)

KEY WORDS: In situ hybridization; RNA; Transmission electron microscopy; Pre-embedding; Saponin; Rat 9G; HeLa; Cytochemistry.

Introduction

In situ hybridization (ISH) at the light microscopic (LM) level has become a widely used method for examining messenger RNA (mRNA) expression and distribution in tissues and single cells. This method, however, is of insufficient resolution to study the localization of individual RNA sequences in relation to cellular ultrastructure. For this purpose, ISH methodologies have been developed that allow visualization of RNAs at the electron microscopic (EM) level. The first EM ISH report by Jacob et al. (1) described a post-embedding method with radioactive labeled probes. The poor localization property of this method was fundamentally overcome by Binder et al. (2) by applying a non-radioactive ISH method. Many EM ISH protocols have since been described. These methods employ post- or pre-embedding approaches and a variety of aldehyde fixations and pre-treatments. In addition, they use different immunological detection systems and reporter molecules, including colloidal gold of different sizes (3–8), enzyme cytochemical precipitates [e.g., peroxidase/diaminobenzidine (DAB)] (9–12), eosin-mediated DAB photo-oxidation (13), and ultra-small gold with silver enhancement (14,15).

A survey of EM ISH studies thus far leads to the general conclusion that an optimal balance between preservation of ultrastructure and hybridization efficiency is difficult to obtain. When a good ultrastructure is present only very abundant RNAs, expressed in specialized or virus-infected cells, are detectable with EM ISH. Less abundant RNAs are detectable only when ultrastructure is compromised by suboptimal fixation or harsh pre-treatments.

In situ hybridization efficiency is determined by the accessibility of RNA targets, *casu quo* penetration of probes and immunochemicals, as well as by retention of RNAs. Extensive cross-linking during primary fixation will favor preservation of ultrastructural morphology, but is contraindicated for accessibility of RNA. The challenge for EM ISH is therefore how to achieve full penetration

[1] Supported by The Netherlands Organization for Scientific Research, Department of Medical Sciences (NWO-MW), Grant no. 900-534-079.
[2] Correspondence to: Merryn V.E. Macville, Dept. of Cytochemistry & Cytometry, Faculty of Medicine, U. of Leiden, Sylvius Laboratories, Wassenaarseweg 72, 2333 AL Leiden, The Netherlands.
[3] Present address: Dept. of Cell Biology and Histology, University of Nijmegen, Nijmegen, The Netherlands.

of probes and immunochemicals without compromising ultrastructural morphology.

In post-embedding techniques, RNA sequences are directly accessible to hybridization reagents at the sectioned surface but are therefore also more susceptible to RNAses. Furthermore, the embedding medium masks most of the internal RNA targets, leading to suboptimal detection efficiency (11,16–18). Even in ultra-thin cryosections, it is difficult to reveal internal targets (11,16,17,19). In principle, higher detection efficiency can be obtained by a pre-embedding approach if, as discussed, full penetration of detection chemicals can be achieved without affecting ultrastructural morphology.

In fixed cells, the plasma membrane, cytoplasmic membranes, and the cross-linked proteinaceous cell matrix constitute the main barriers to ISH reagents. Treatments to increase the penetration of these reagents are often targeted to these barriers. Recently we evaluated several aldehyde fixatives and treatments for their effects on reagent penetration and morphology in a combined light (LM) and transmission electron microscopic (TEM) study (20). We showed that digestion of the proteinaceous cell matrix by, e.g., pepsin indeed improved reagent penetration but that the ultrastructural morphology was disrupted to an unacceptable extent. Targeting the lipid component of cell membranes by treatments with organic solvents, such as ethanol and xylene, also proved too harsh for preservation of subcellular integrity.

Several pre-embedding EM studies for immunolocalization of antigens have evaluated the use of detergents such as Triton X-100, Nonidet P40, saponin, digitonin, or bacterial toxins for their permeabilizing effects (for reviews see 21,22). In most of these studies saponin was the permeabilizing agent of choice (23–25). In addition, for LM ISH the benefit of saponin as a permeabilizing agent has been reported (26). Saponin treatment does not affect or only minimally affects the ultrastructure of aldehyde-fixed cells and facilitates the penetration of detection reagents, which is explained by the fact that extraction of the cholesterol component leads to sufficiently large "holes" to allow diffusion of antibodies through membranous structures and that the retention of phospholipids and membrane proteins provides sufficient ultrastructural features on TEM examination (27–31).

Although removal of the membrane barriers by saponin permeabilization facilitates reagent penetration, this does not necessarily mean that the accessibility of RNA targets is improved. Depending on the extent of aldehyde fixation, the cross-linked proteinaceous matrix may still limit the penetration of probe, antibody, or both. It was therefore of interest to study the influence of saponin permeabilization on ISH signals and ultrastructural morphology in relation to formaldehyde and glutaraldehyde fixations of various cross-linking strengths. Before processing the specimens for TEM, we monitored the effects of saponin and fixations on morphology and ISH signal by reflection-contrast microscopy (RCM). We have previously shown that the preservation of ultrastructural morphology can be predicted to a large extent from RCM interference patterns (20). In addition, RCM provides a means to assess ISH signal intensity by the reflection properties of the DAB precipitate (32). Therefore, RCM evaluation of ISH results allowed rapid establishment of optimal fixation and permeabilization conditions for EM ISH. Furthermore, we compared peroxidase/DAB detection with ultra-small gold/silver enhancement for their use in the EM ISH technique.

Materials and Methods

Cell Culture. Rat 9G fibroblasts and HeLa cells were grown to subconfluency on polystyrene 6-well culture plates (Type 3506; Costar Europe, Badhoevedorp, The Netherlands) or sterilized glass slides in Dulbecco's minimal essential medium supplemented with 5% (v/v) fetal calf serum at 37°C in a 5% CO_2 atmosphere. Immediate early (IE) mRNA expression was induced in 20–30% of the rat 9G cell population by addition of 50 μg/ml cycloheximide (Sigma; St Louis, MO) for 5 hr at 37°C to exponentially growing cells (33).

Nucleic Acids and Labeling. For detection of rRNA, a pGEM plasmid containing a 2.1 KB insert specific for the 3' site of human 28S rRNA was used (34,35). For detection of human elongation factor (HEF) mRNA in HeLa cells, a plasmid probe containing HEF-1 cDNA has been used (36). For detection of IE mRNA in rat 9G cells, a genomic plasmid probe containing the 5 KB SphI-SalI fragment of the transfected human cytomegalovirus (HCMV) IE region has been used (33). As negative control probes, plasmids were used containing either a satellite-III sequence of the 1q12 region of human chromosome 1 (37) or 1 KB cDNA sequence of the caudodorsal cell hormone gene of the pond snail *Lymnaea stagnalis* (38). Probes were labeled with digoxigenin-11-dUTP (Boehringer–Mannheim; Mannheim, Germany) by nick-translation and purified by Sephadex G50 (Pharmacia Biotech; Woerden, The Netherlands) gel filtration. Fragment length of labeled probes was 100–400 BP as estimated by Southern blotting.

Fixations and Pre-treatments. After culturing, cells were washed briefly with Ringer's PBS (1.4 mM Na_2HPO_4/NaH_2PO_4, 150 mM NaCl, 4 mM KCl, 2.2 mM $CaCl_2$, pH 7.4) at room temperature (RT) and fixed for 30 min at RT in 1% (w/v) formaldehyde (FA) or 1% FA in combination with 0.05% or 0.5% (v/v) glutaraldehyde (GA, EM grade; Fluka Chemie; Buchs, Switzerland) in 0.15 M $NaHCO_3$, pH 8.6 (39). Formaldehyde solutions were prepared from paraformaldehyde shortly before use. After fixation, cells were consecutively permeabilized in 0.1% saponin (Fluka)/PBS (136 mM NaCl, 2.7 mM KCl, 8.4 mM Na_2HPO_4, 0.9 mM KH_2PO_4, pH 7.4) for 30 min at RT, post-fixed in 1% FA/PBS for 10 min, and incubated with 1% (w/v) hydroxyl ammonium chloride (Sigma)/PBS for 10 min to quench fixation-induced free aldehydes. The cells were rinsed in RNAse-free PBS between the incubation steps. Alternatively, saponin permeabilization and post-fixation were omitted from the protocol.

Pre-embedding In Situ Hybridization. The pre-embedding EM ISH procedure was performed on polystyrene 6-well culture plates. The hybridization conditions were based on the LM ISH protocol previously described for cultured cells (40,41). A hybridization mixture, consisting of 60% deionized formamide, 2 × SSC (0.3 M NaCl, 0.03 M sodium citrate), 25 mM NaH_2PO_4, 10 mM EDTA, pH 7.4, 100 μg/ml herring sperm DNA, 100 μg/ml yeast tRNA, and 5 ng/μl labeled probe, was denatured at 80°C for 3 min and a total volume of 10 μl was used under a 20 × 20-mm^2 piece of Parafilm. The hybridization was allowed to proceed for 16 hr at 37°C in a moist chamber. Three post-hybridization washes of 10 min each were performed in 60% formamide/2 × SSC at 37°C. Negative controls consisted of hybridizations without probe or with a nonspecific probe (mock solution), pre-treatment of cells with RNAse-A (100 μg/ml 2 × SSC) before hybridization for 30 min at 37°C, and hybridizations on cells that do not express the relevant RNA sequence.

Hybrid Detection by Immunoperoxidase/DAB. After stringent washes (40,41), digoxigenin-labeled RNA–DNA hybrids were detected with peroxidase-conjugated anti-digoxigenin $F(ab)_2$ fragments (Boehringer–Mannheim) diluted 1:250 in a buffer containing 600 mM NaCl, 100 mM Tris-

HCl, pH 7.4, 0.5% (w/v) blocking reagent (Boehringer–Mannheim), and 0.1% saponin. After incubation for 2 hr at 37°C in a moist chamber, cells were rinsed in 150 mM NaCl, 100 mM Tris-HCl, 0.1% saponin, pH 7.4, three times for 10 min. The immunodetection buffers contained saponin only if the cells were treated with saponin after primary fixation. For visualization of the peroxidase label, cells were incubated at RT for 20 min in the dark with 0.5 mg/ml 3,3'-diaminobenzidine tetrahydrochloride (DAB; Sigma) in 50 mM Tris-HCl, pH 7.4, containing 10 mM imidazole and 0.005% (v/v) H_2O_2. Cells were post-fixed in 2% GA/$NaHCO_3$ for 10 min and subsequently in 1% OsO_4/Millonig's phosphate (0.16 M NaH_2PO_4/0.63 M NaOH, pH 7.3) for 30 min at 4°C before RCM monitoring or TEM embedding procedures.

Hybrid Detection by Ultra-small Gold and Silver Enhancement. After stringent washes, cells were washed in PBS and incubated for 30 min at 37°C in high-salt PBS (586 mM NaCl, 2.7 mM KCl, 8.4 mM Na_4HPO_4, 0.9 mM KH_4PO_4, pH 8.0) supplemented with 0.1% acetylated BSA (Aurion; Wageningen, The Netherlands), 0.1% cold water fish skin gelatin, and 0.1% saponin. Anti-digoxigenin $F(ab)_2$ fragments conjugated to ultra-small gold particles (≈0.8 nm; Aurion) were diluted 1:100 in the same buffer. After overnight incubation at 37°C in a moist chamber, specimens were washed in incubation buffer six times for 15 min, in PBS three times for 5 min, and in double-distilled water six times for 5 min. After post-fixation in 2% GA/$NaHCO_3$ for 10 min and 1% OsO_4/Millonig's phosphate for 30 min at 4°C, silver enhancement according to Danscher (42) was performed for 45 min. Cells were then further processed for microscopy.

Embedding and Ultramicrotomy. Cells were embedded in epon resin for cross-sections as described previously (20). For ultra-thin sections parallel to the culture dish, regular Beem capsules without a cap were filled with epon and placed inverted over resin-infiltrated cells. After polymerization for 48 hr at 60°C, the blocks were broken from the polystyrene wells, exposing flat-embedded cells at their surfaces. Ultra-thin sections (60–90 nm) were cut with a diamond knife on a Reichert Ultracut E ultramicrotome and mounted on carbon-coated parlodion films on copper grids.

Microscopy. The effects of fixation and pre-treatments on ISH signals and cell morphology were monitored with a Leitz Orthoplan microscope (Ernst Leitz; Wetzlar, Germany) adapted for reflection-contrast microscopy (32,43). RCM micrographs were taken on 100 ASA daylight colorfilm. For TEM, we used a Philips EM 410LS operating at 60 or 80 kV.

Results

RCM Observations

On the basis of RCM interference patterns from cells devoid of ISH signal (i.e., rat 9G cells not expressing IE mRNA and HeLa cells hybridized in mock solution), we first examined the morphology of the cells exposed to different fixatives and pre-treatments (Table 1). Previously we have shown that ultrastructural morphology of rat 9G cells can be predicted from such interference patterns to a large extent (20). The criteria defined for rat 9G cells can also be applied to HeLa cells (unpublished results). When rat 9G cells were fixed with 1% FA without GA, they displayed concentrically arranged colors occupying about 20% of the cell surface, and a white-gray periphery. This pattern predicts a fairly well-preserved ultrastructural morphology. An identical color pattern was observed when such fixed cells were treated with saponin (Figure 1A). Cells fixed with 1% FA/0.05% GA or 1% FA/0.5% GA showed concentrically arranged colors over 40–60% of the cell surface, both in the presence (Figures 1B and 1C) and the absence of saponin treatment, predicting a well-preserved ultrastructural morphology.

Second, we examined the effect of saponin pre-treatment on ISH signal intensity in relation to the fixatives used. RCM has proven to be very sensitive for detection of very small amounts of DAB signal, which appears as white spots. Hereby, RCM extended the range for ISH signal detection. However, DAB loses its reflection properties, owing to absorption of incident light, when present in very large amounts (44). In that case, by examining the same image field by brightfield LM, DAB is clearly visible as a brown precipitate. In the results presented here, brightfield LM was used in addition to RCM.

For all fixatives tested, the 28S rRNA ISH signal intensity in the cytoplasm of both rat 9G and HeLa cells increased considerably as a result of saponin treatment (Table 2). The nucleoli, however, remained devoid of 28S rRNA ISH signal, even after 1% saponin treatment for 2 hr (data not shown).

IE mRNA is differentially expressed within a rat 9G population (33), and therefore a favorable effect of saponin could not only lead to an increase in IE mRNA ISH signal intensity but also to an increase of the percentage of detected IE mRNA-expressing cells. Indeed, saponin treatment resulted in a higher detection percentage of IE-mRNA-positive cells as well as stronger signals (Table 3). Figures 1A–1C show representative hybridization results for IE mRNA on rat 9G cells as shown by RCM for fixation with 1% FA, 1% FA/0.05% GA, and 1% FA/0.5% GA, respectively. IE mRNA was found in the cytoplasm and in one large spot in the nucleus, which probably represents the transcription site of the IE gene. Nuclear signals that could not be observed clearly by RCM were clearly visible when the same image field was examined by brightfield LM (data not shown).

The type of fixation proved to have a direct influence on the ISH signal intensity in saponin-treated cells. The strongest ISH signals were found in 1% FA-fixed cells for all RNA targets. The in-

Table 1. *RCM and TEM observations of the morphology of cultured rat 9G and HeLa cells after ISH in the absence and presence of saponin pre-treatment in correlation with primary fixation*

	Without saponin		With saponin	
	RCM[a]	TEM[b]	RCM[a]	TEM[b]
1% formaldehyde	+	+	+	–
1% formaldehyde/0.05% glutaraldehyde	+ +	+ +	+ +	+ +
1% formaldehyde/0.5% glutaraldehyde	+ + +	+ +	+ + +	+ +

[a] Reflection-contrast microscopy. + + +, concentric colors over 60% of the cell; + +, 40% concentric colors; +, 20% concentric colors.
[b] Transmission electron microscopy. + +, well-preserved ultrastructure; +, fairly well-preserved ultrastructure; –, poor ultrastructure.

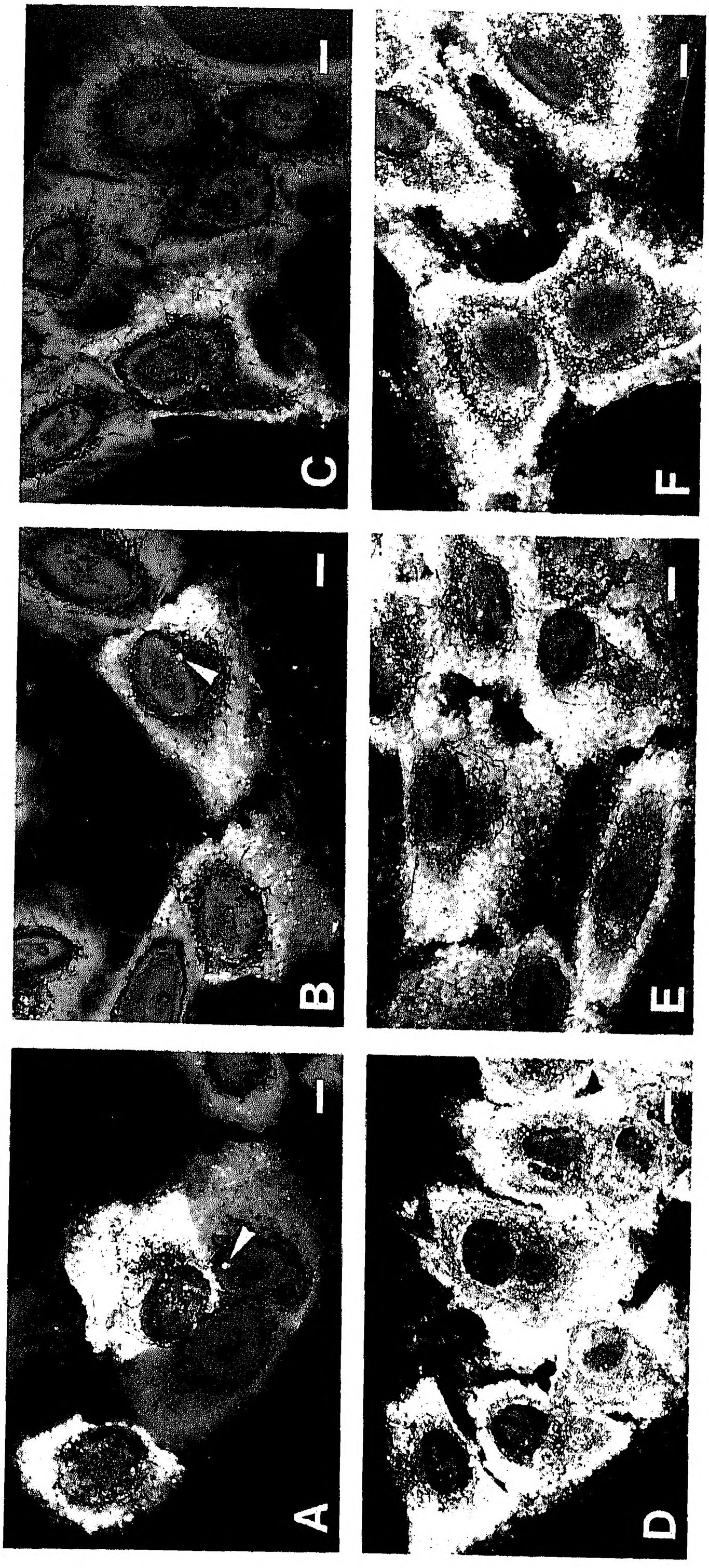

Figure 1. RCM images of rat 9G cells fixed with (**A,D**) 1% FA, (**B,E**) 1% FA/0.05% GA and (**C,F**) 1% FA/0.5% GA, permeabilized with 0.1% saponin, and hybridized. (**A–C**) Different intensity levels of IE mRNA signals are present in a subpopulation of the cells over the entire cytoplasm. The white DAB spot in the nucleus (arrowheads) is not visible in all IE mRNA-expressing cells (see text). From IE mRNA non-expressing cells, interference color patterns can be examined. (**D–F**) 28S rRNA ISH signals are present over the entire cytoplasm of all cells but not in nucleoli. Bars = 5 μm.

Table 2. *RCM and TEM observations of ISH signals for 28S rRNA in rat 9G and HeLa cells in the absence and presence of saponin pre-treatment in correlation with primary fixation*

	Without saponin		With saponin	
	RCM[a]	TEM[b]	RCM[a]	TEM[b]
1% formaldehyde	+	−	+ + +	+ + +
1% formaldehyde/0.05% glutaraldehyde	±	−	+ +	+ +
1% formaldehyde/0.5% glutaraldehyde	±	−	+	±

[a] Reflection-contrast microscopy. + + +, very strong DAB; + +, strong DAB; +, clearly visible DAB spots; ±, weak DAB spots.
[b] Transmission electron microscopy. + + +, very strong DAB; + +, strong DAB; ±, a few DAB spots; −, no DAB visible.

Table 3. *RCM and TEM observations of ISH signals for IE mRNA in rat 9G cells in the absence and presence of saponin pre-treatment in correlation with primary fixation*

	Without saponin		With saponin	
	RCM[a]	TEM[b]	RCM[a]	TEM[b]
1% formaldehyde	+	−	+ + +	+ + +
1% formaldehyde/0.05% glutaraldehyde	−	−	+ +	+ +
1% formaldehyde/0.5% glutaraldehyde	−	−	+	±

[a] Reflection-contrast microscopy. + + +, approximately 20% positive cells, many with very strong DAB; + +, approximately 20% positive cells, a few with very strong DAB; +, approximately 10% positive, none with very strong DAB; −, no signals.
[b] Transmission electron microscopy. + + +, in cytoplasm very strong DAB and in nucleus very strong main spot with many smaller spots; + +, in cytoplasm strong DAB spots and in nucleus very strong main spot with a few smaller spots; ±, in cytoplasm a few DAB spots and in nucleus main spot clearly visible; −, no DAB visible.

Table 4. *RCM and TEM observations of ISH signals for HEF mRNA in HeLa cells in the absence and presence of saponin pre-treatment in correlation with primary fixation*

	Without saponin		With saponin	
	RCM[a]	TEM[b]	RCM[a]	TEM[b]
1% formaldehyde	±	−	+ +	+ +
1% formaldehyde/0.05% glutaraldehyde	−	−	+ +	+ +
1% formaldehyde/0.5% glutaraldehyde	−	−	−	−

[a] Reflection-contrast microscopy. + +, strong DAB; ±, weak DAB speckles; −, no DAB visible.
[b] Transmission electron microscopy. + +, strong DAB spots; −, no DAB visible.

tensity of ISH signals gradually decreased when the GA concentration in the fixative increased (Tables 2, 3, and 4). For ISH detection efficiency of HEF mRNA in HeLa cells, the favorable effect of saponin was also evident (Table 4). HEF mRNA was exclusively localized in the cytoplasm of 1% FA- and 1% FA/0.05% GA-fixed HeLa cells only when they were permeabilized with saponin. However, detection of HEF mRNA was not possible when cells were fixed with 1% FA/0.5% GA, even when the cells were permeabilized with saponin. Clearly, the effect of saponin on RNA detection efficiency is less beneficial as the extent of cross-linking increases.

TEM Observations

In accord with the predictions made on the basis of RCM interference color patterns, the ultrastructural architecture of HeLa and rat 9G cells fixed with 1% FA/0.05% GA or 1% FA/0.5% GA was visibly unaltered after saponin treatment and subsequent hybridization and immunodetection (Table 1). Also in accord with the RCM predictions, cells fixed with 1% FA but not treated with saponin showed poorer intracellular architecture compared to cells fixed with GA-containing fixatives (Table 1). However, RCM did not predict the deterioration of ultrastructural morphology of 1% FA-fixed cells as observed after saponin treatment (Figures 2A, 3, and 5).

For all fixatives tested, 28S rRNA ISH signals that were observed in RCM but not in TEM when saponin pre-treatment was omitted were clearly visible in TEM when cells were pre-treated with saponin (Table 2). Cross-sections of 1% FA-fixed cells demonstrated full penetration of 28S rRNA ISH signals into the cytoplasm (Figure 2A), and parallel sections demonstrated a homogeneous cytoplasmic distribution (Figure 3). As expected from RCM (and bright-field LM) results of 28S rRNA ISH, nucleolar signals were not visible. In 1% FA-fixed cells, it was not possible to exactly localize 28S rRNA sequences to cell components because of the poor morphological features of the cytoplasm.

A good balance between preservation of ultrastructural morphology and 28S rRNA ISH signal was obtained when cells were primarily fixed in 1% FA/0.05% GA and then treated with saponin. 28S rRNA ISH signals were clearly present over the rough endoplasmic reticulum and ribosomes throughout the entire cytoplasm of rat 9G (Figure 2B) and HeLa cells (Figure 4A). In cells fixed in 1% FA/0.5% GA, the ISH detection efficiency for 28S rRNA

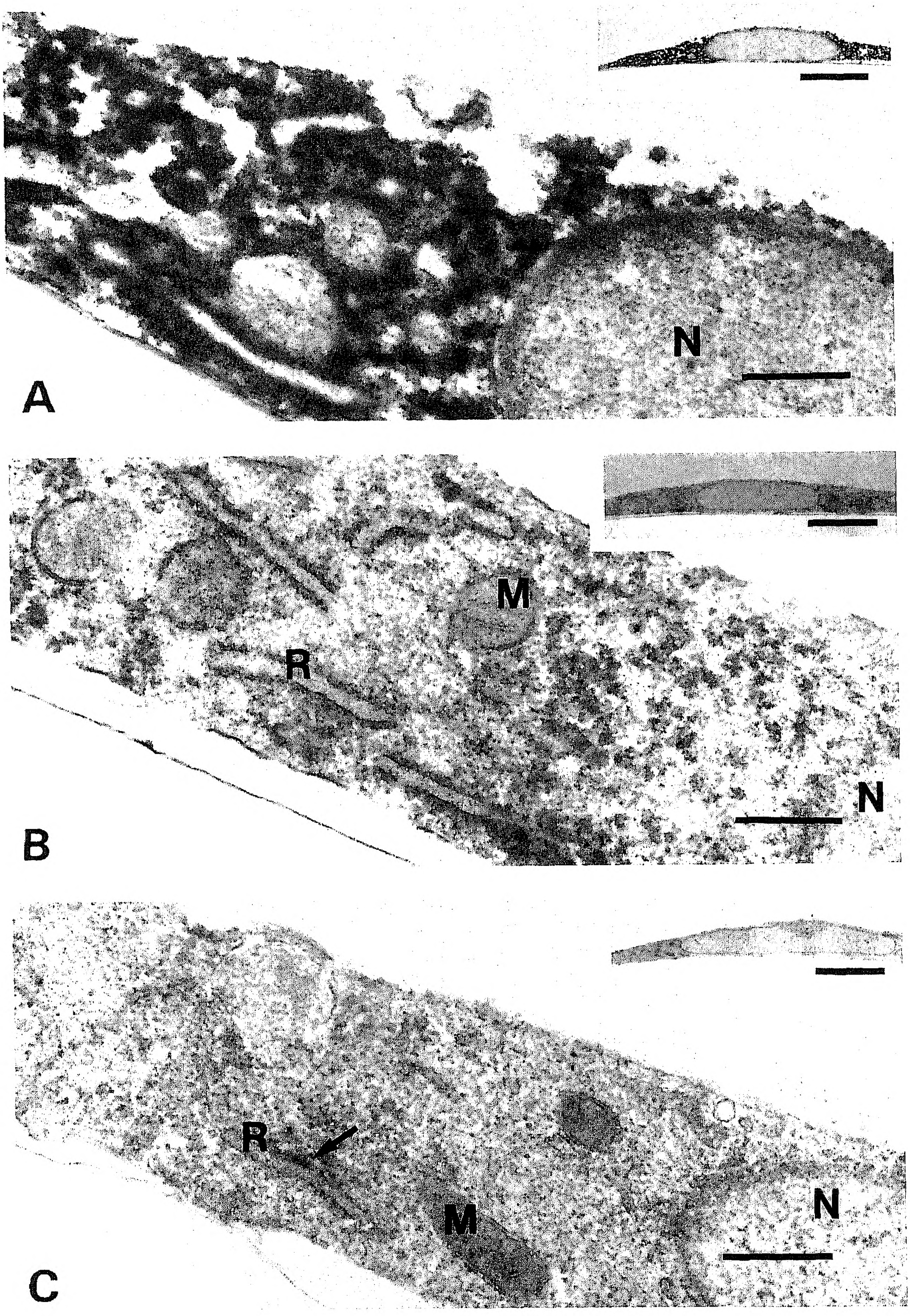

Figure 2. TEM images of cross-sections of rat 9G cells at low magnification (**insets**) and high magnification that were permeabilized with 0.1% saponin and hybridized with 28S rRNA. (**A**) Cells fixed with 1% FA show damaged cell architecture but very strong DAB signal. (**B**) Cells fixed with 1% FA/0.05% GA show DAB fully penetrated into and homogeneously distributed over the cytoplasm, revealing a clear association of 28S rRNA with ribosomes. (**C**) Cells fixed with 1% FA/0.5% GA show a few DAB signals (arrow) and well-preserved ultrastructural morphology. N, nucleus; R, rough endoplasmic reticulum; M, mitochondrion. Bars = 0.5 μm; **insets** = 5 μm.

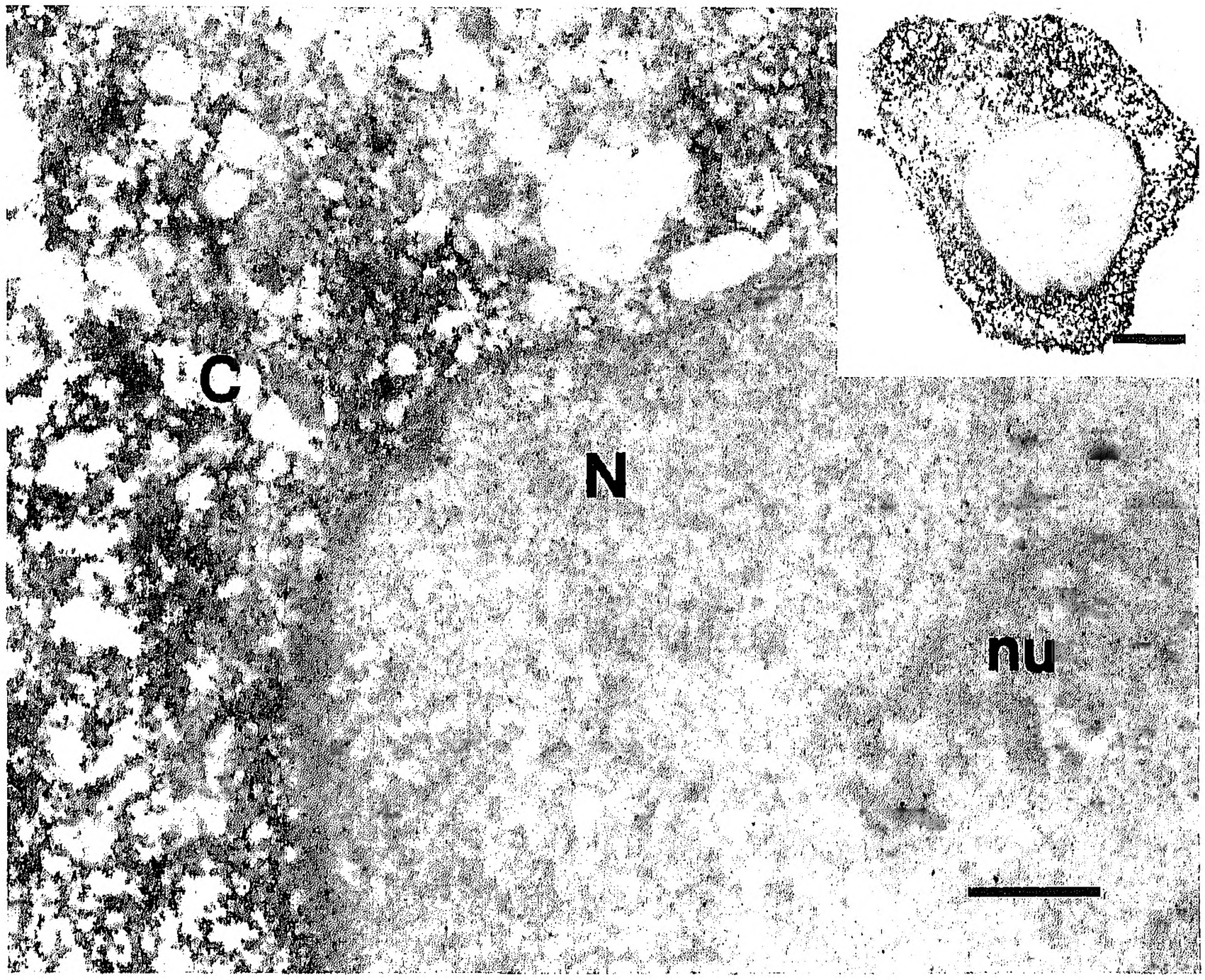

Figure 3. TEM image of a 1% FA-fixed rat 9G cell permeabilized with 0.1% saponin and hybridized for 28S rRNA. DAB signals are homogeneously distributed over the cytoplasm (C) but not in the nucleus (nu). N, nucleus. Bar = 1 μm; **inset** = 5 μm.

was still low, and therefore only a few DAB spots were clearly discernible from cell constituents (Figure 2C).

The observed localization pattern of IE mRNA at the TEM level in the cytoplasm and nucleus of rat 9G cells was also strongly influenced by the extent of cross-linking during primary fixation. In 1% FA-fixed and saponin-treated rat 9G cells, IE mRNA was found homogeneously over the cytoplasm and in one large nuclear spot, which was often located close to or in contact with the nuclear membrane. In addition, many smaller spots were observed dispersed over the nucleus but not over the nucleolus (Figure 5). In cells fixed with 1% FA/0.05% GA, IE mRNA was localized in the cytoplasm in many foci associated with ribosomes. In the nucleus, again one large spot was observed, but in contrast to the 1% FA-fixed cells, the hybridization spots around it were considerably smaller and fewer in number (Figure 6). With either fixative, 20–30% of the rat 9G cell population displayed IE mRNA expression. This result is in agreement with ISH results observed with RCM (Table 3).

IE mRNA expression in rat 9G cells is high owing to a strong, inducible promoter-enhancer element in the transfected HCMV-IE transcription unit. To investigate whether less abundant mRNAs can be detected at the EM level, we performed ISH for detection of HEF housekeeping gene transcripts in HeLa cells (Table 4). In 1% FA- and 1% FA/0.05% GA-fixed HeLa cells that were subsequently treated with saponin, HEF mRNA was found in many foci dispersed over the cytoplasm. Ribosomes of the rough endoplasmic reticulum appeared to be devoid of label, which implies that HEF mRNA is associated with free or cytoskeleton-bound ribosomes. Nuclei were always devoid of label (Figure 7).

Hybrid Detection by Ultra-small Gold and Silver Enhancement

We investigated whether permeabilization with saponin allows detection of intracellular targets by ultra-small gold conjugates and Danscher silver enhancement (42). In HeLa cells, detection of 28S rRNA–DNA hybrids resulted in much lower signal intensities with ultra-small gold/silver enhancement than with peroxidase/DAB in both LM, RCM, and TEM (compare Figures 4A and 4B). After silver enhancement, very small particles were observed next to very large particles (>200 nm). Moreover, as a result of ultra-thin sectioning, large gold/silver particles caused local disruption of cell ultrastructure. In control experiments, cells that were hybridized with mock solution showed low background labeling over the nucleus, and when the gold conjugate was omitted cells showed no labeling (data not shown), proving that silver enhancement was specific for gold particles.

Specificity of ISH Signals

No ISH signals were obtained when hybridization was preceded by an RNAse-A treatment or when ISH experiments were performed using nonspecific probes. Moreover, nuclear ISH signals were obtained without in situ denaturation of nuclear DNA, implying that RNA was detected and not DNA.

In rat 9G cell populations, 20–30% of the cells expressed IE mRNA after cycloheximide induction. This is in agreement with

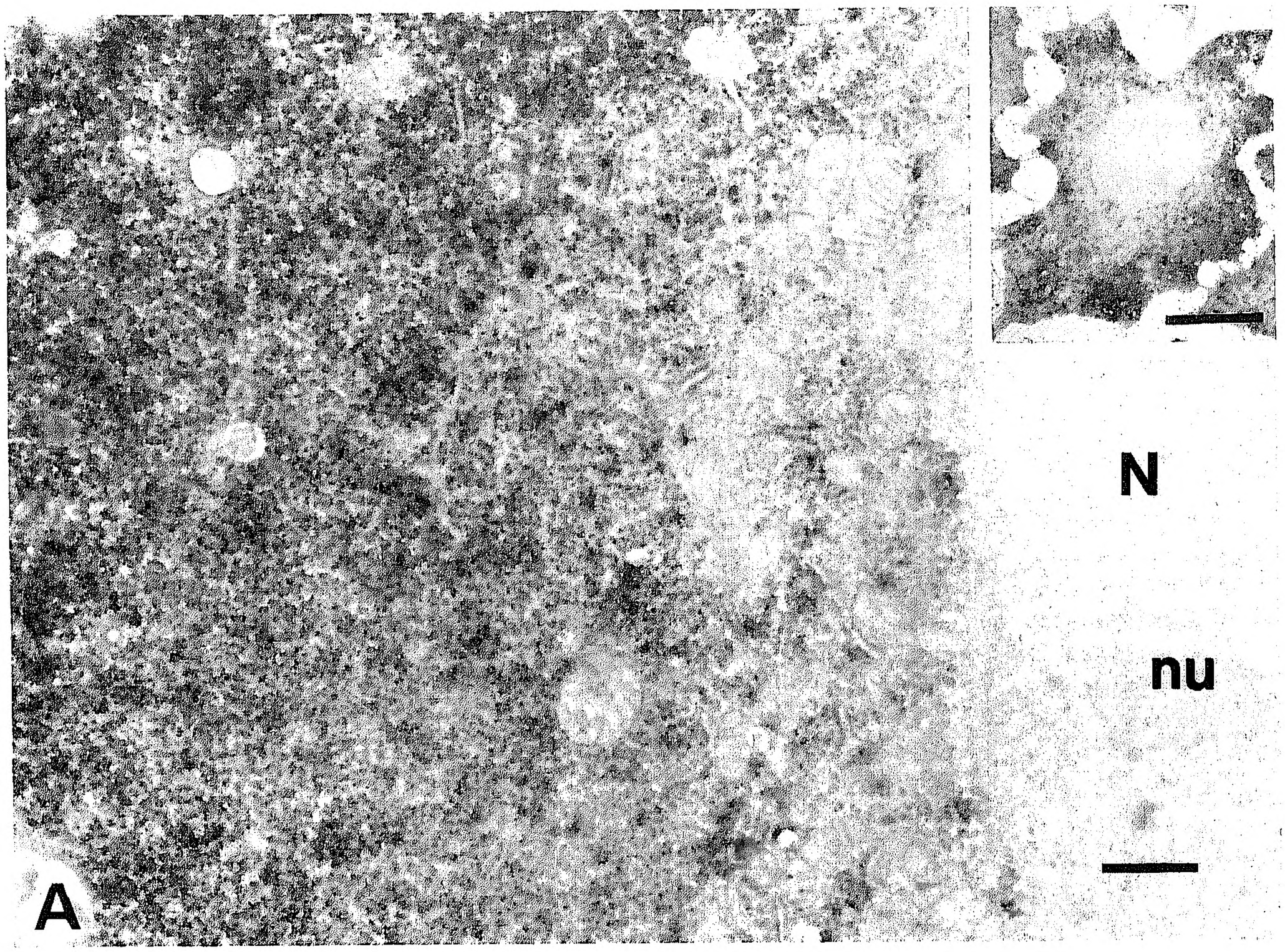

Figure 4. TEM images of HeLa cells fixed with 1% FA/0.05% GA and permeabilized with 0.1% saponin, showing well-preserved cellular ultrastructure. (**A**) Detection of 28S rRNA–DNA hybrids using peroxidase/DAB, and (**B**) using ultra-small gold conjugates and silver enhancement. Arrows indicate damage of cell structure caused by large gold/silver particles during sectioning. N, nucleus; nu, nucleolus. Bars =1 μm; **insets** = 10 μm.

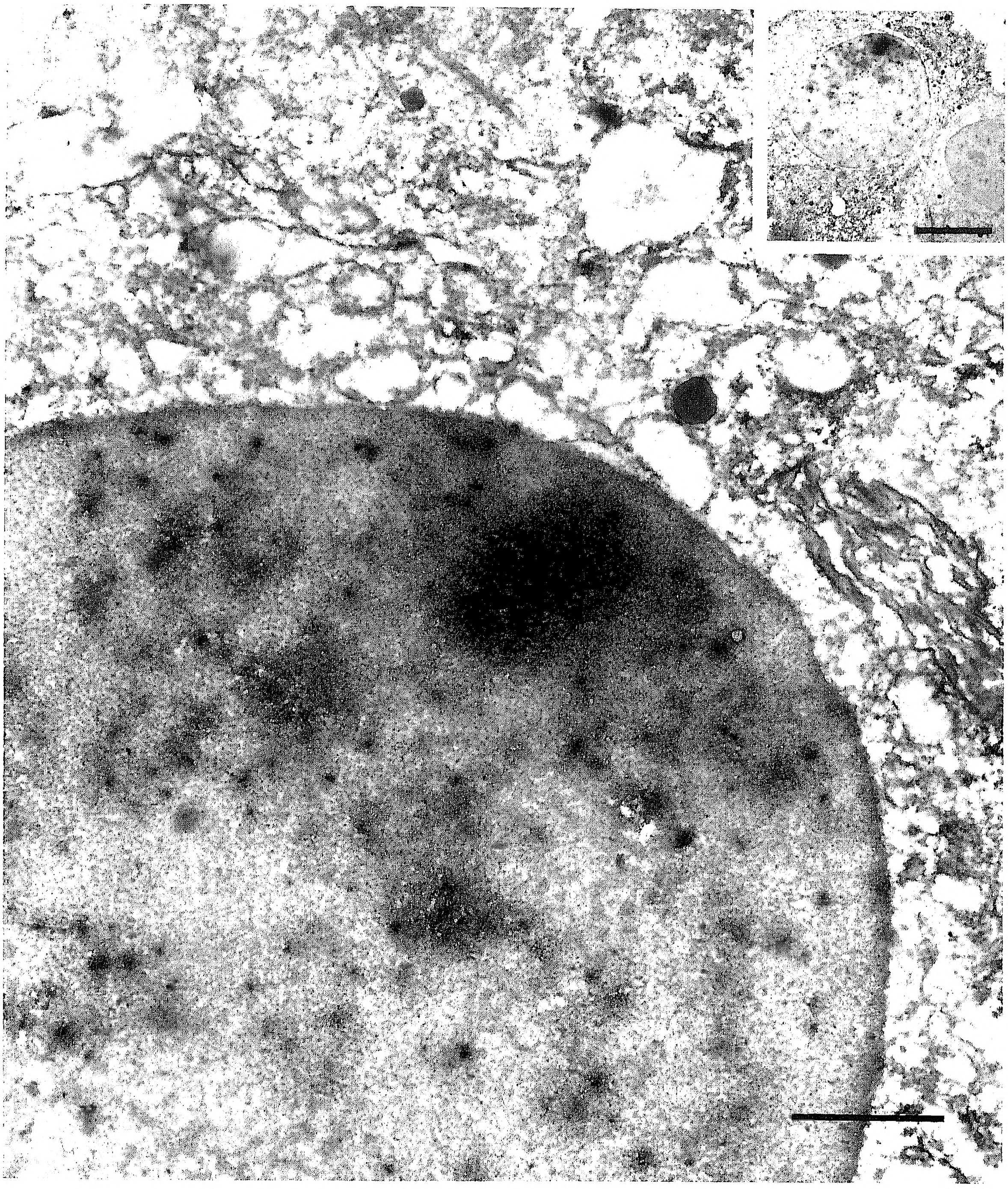

Figure 5. TEM image of a 1% FA-fixed rat 9G cells permeabilized with 0.1% saponin and hybridized for IE mRNA. IE mRNA is present over the entire cytoplasm. In the nucleus, one large nuclear spot close to the nuclear membrane is surrounded by many small spots. IE mRNA non-expressing cells were devoid of DAB (lower right corner of **inset**). Bar = 2 μm; **inset** = 10 μm.

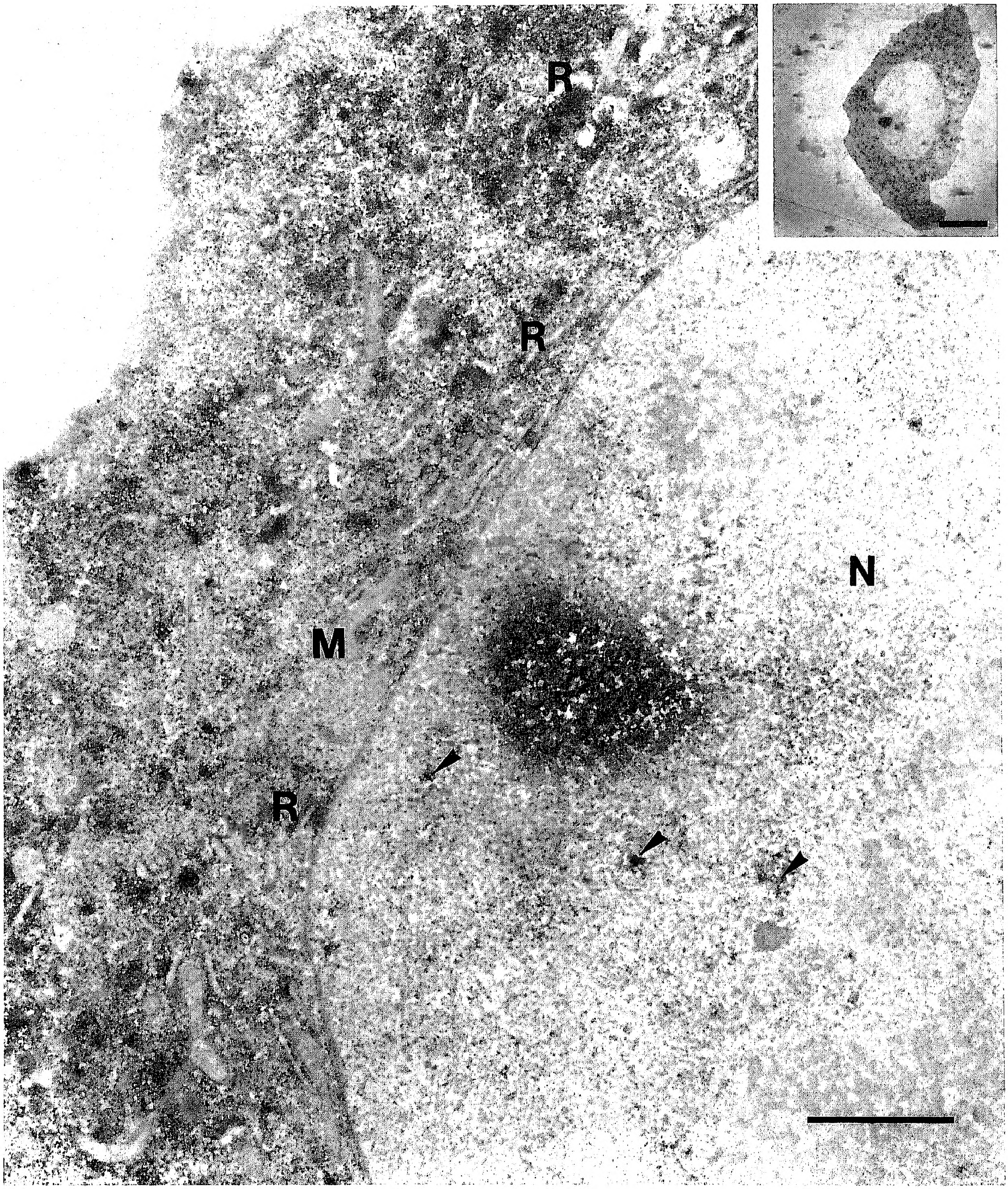

Figure 6. TEM image of a 1% FA/0.05% GA-fixed rat 9G cell permeabilized with 0.1% saponin and hybridized for IE mRNA. IE mRNA is localized in the cytoplasm and associated with free and rough endoplasmic reticulum (R)-bound ribosomes. The large nuclear spot close to the nuclear membrane is surrounded by a few smaller spots (arrowheads). N, nucleus; M, mitochondrion. Bar = 2 μm; **Inset** = 10 μm.

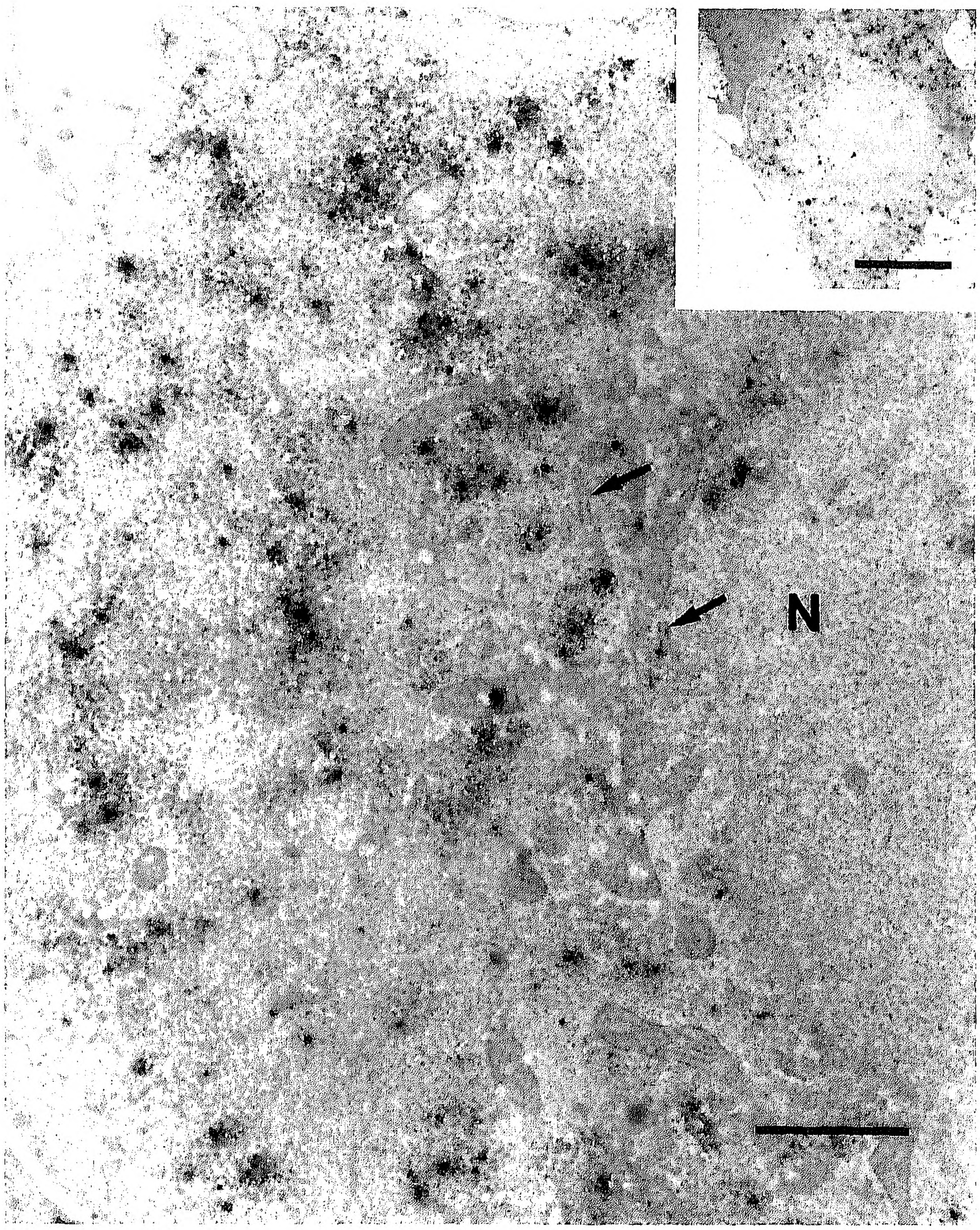

Figure 7. Ultrastructural localization of HEF mRNA in HeLa cell fixed with 1% FA/0.05 GA and permeabilized with 0.1% saponin demonstrates DAB spots in the cytoplasm. Ribosomes associated with the endoplasmic reticulum (arrows) are devoid of label. N, nucleus. Bar = 2 μm; **inset** = 10 μm.

IE protein expression studies by Boom et al. (33). Furthermore, the presence of IE mRNA non-expressing cells provides a strong internal specificity control.

Discussion

A reiterative problem in the development of pre-embedding EM ISH techniques is to design fixation and pre-treatment conditions such that all RNA molecules are accessible to probes and immunochemicals and ultrastructural morphology is preserved. Most strategies for improving reagent penetration resulted in insufficient preservation of ultrastructure or suboptimal detection efficiency. This study shows that saponin treatment of aldehyde-fixed cells can significantly contribute to reaching the aim of good penetration of ISH reagents in ultrastructurally well-preserved cells. Saponin exclusively removes cholesterol molecules from lipid-containing structures (31), leaving stable holes (28) large enough for penetration of nucleic acids (45) and peroxidase or gold-conjugated $F(ab)_2$ antibodies. As shown in this study, even in the presence of a saponin treatment the extent of aldehyde cross-linking of cellular proteins has a strong influence on both ultrastructure and reagent penetration. Actually, no conditions were found in which reagent penetration and good ultrastructural morphology were obtained for all cell compartments.

In 1% FA-fixed and saponin-treated cells, the cytoplasmic ultrastructure is suboptimal, whereas the nuclear morphology is good. As evidenced by 28S rRNA ISH, cytoplasmic reagent penetration is good but nucleolar regions are still not accessible. Furthermore, the presence of intense IE mRNA signals in the nuclei proved that reagent penetration into the nucleoplasm is good also.

A comparison between the results obtained with 1% FA and the stronger cross-linking fixative 1% FA/0.05% GA demonstrates that balancing reagent penetration on the one hand and preservation of ultrastructure on the other is indeed subtle, even in the presence of saponin treatment. For the cytoplasm, the stronger fixative provides a better ultrastructure, but a weaker ISH signal intensity (compare Figures 2A and 2B). Because 28S rRNA signal is present throughout the cytoplasm and because reagents even reach the nucleoplasm (as evidenced by the main IE mRNA signal in the nuclei of rat 9G cells) under 1% FA/0.05% fixation conditions, we infer that local accessibility limitations account for the reduced cytoplasmic 28S rRNA signals.

The ultrastructure of cells fixed with the strongest cross-linking fixative (1% FA/0.5% GA) and treated with saponin is good, but the absence of HEF mRNA signals and the weak ISH cytoplasmic 28S rRNA and IE mRNA signals indicate that with this fixative hybridization efficiencies are too low to be of use for EM ISH; the balance has shifted too much toward preservation of ultrastructure.

The choice of fixation for pre-embedding EM ISH should be based on the demands of the RNA distribution study at hand. Those aiming at visualizing cytoplasmic RNA distribution patterns should preferably use 1% FA/0.05% GA, whereas those aiming at nucleoplasmic patterns should use 1% FA.

Ultrastructural localization studies for nucleolar RNA and DNA thus far have employed post-embedding EM ISH techniques, because nucleotide sequences at the sectioned surface are readily detected. The detection efficiency, however, is low and this may underlie the fierce dispute about the precise localization of active ribosomal genes (46–49). In pre-embedding EM ISH, nucleolar targets have been detected only after severely damaging ultrastructural morphology by 4% FA/acetic acid fixation and pepsin digestion (20), or after nuclear matrix preparation and DNAse-I digestion (50). Apparently, access to nucleolar RNA targets of intact cells is hampered by compact entwinement of RNA, DNA, and (cross-linked) protein.

A number of observations were made in this study that relate to functional (ultrastructural) localization of the mRNA ISH signals. In 1% FA/0.05% GA-fixed, saponin-treated HeLa cells, a correlation with a subpopulation of ribosomes was seen for HEF mRNA. This mRNA codes for a protein that functionally localizes in the cytoplasm. In accord with the consensus theory that such proteins are synthesized at free or cytoskeleton-bound ribosomes, we observed HEF mRNA signals only in association with ribosomes throughout the cytoplasm, and not with those of the endoplasmic reticulum. Although the same correlation was expected in rat 9G cells for IE mRNA, which codes for a nuclear protein, it was actually not found: both free and endoplasmic reticulum-bound ribosomes showed IE mRNA signals. The biological implications of the IE mRNA ISH signals observed in the nucleus will be discussed elsewhere (51; and Macville et al., manuscript submitted for publication).

In our hands, the ISH results obtained with the ultra-small gold detection system were inferior to the immunoperoxidase/DAB system. The weaker ISH signals are due to suboptimal silver enhancement rather than to limited penetration of ultra-small gold particles into the cell interior. Therefore, silver enhancement protocols (52,53) that claim better control over the efficiency and uniformity should be tested for the application of ultra-small gold reagents in pre-embedding EM ISH.

In conclusion, we established a reliable, efficient, and sensitive protocol for ISH detection of RNA at the EM level in cultured cells with ultrastructurally well-preserved morphology, by using mild fixation and saponin permeabilization. With this technique, topographical information can be obtained which will contribute to knowledge about nuclear processes, such as mRNA transcription, maturation, and transport, as well as about cytoplasmic processes involving RNA.

Acknowledgments

We are grateful to Dr R. Boom for the gift of rat 9G cells, L.D.C. Verschragen for excellent electron micrographs, F. Van de Rijke and J. Van der Meulen for technical support, and Dr H.K. Koerten and Prof Dr H.J. Tanke for meaningful discussion.

Literature Cited

1. Jacob J, Todd K, Birnstiel ML, Bird A. Molecular hybridization of 3H-labelled ribosomal RNA with DNA in ultrathin sections prepared for electron microscopy. Biochim Biophys Acta 1971;228:761
2. Binder M, Tourmente S, Roth J, Renaud M, Gehring WJ. In situ hybridization at the electron microscopic level: localization of transcripts on ultrathin sections of Lowicryl K4M-embedded tissue using biotinylated probes and protein A-gold complexes. J Cell Biol 1986;102:1646
3. Harris N, Croy RRD. Localization of mRNA for pea legumin: in situ hybridization using a biotinylated cDNA probe. Protoplasma 1986; 130:57
4. Webster HF, Lamperth L, Favilla JT, Lemke G, Tesin D, Manuelidis L. Use of biotinylated probe and in situ hybridization for light and electron microscopic localization of P0 mRNA in myelin-forming Schwann cells. Histochemistry 1987;86:441
5. Wolber RA, Beals TF, Maassab HF. Ultrastructural localization of *Herpes simplex* virus RNA by in situ hybridization. J Histochem Cytochem 1989;37:97
6. Silva FG, Lawrence JB, Singer RH. Progress towards ultrastructural identification of individual mRNAs in thin section: myosin heavy chain mRNA in developing myotubes: In Bullock GR, Petrusz P, eds. Techniques in immunocytochemistry. Vol 4. London: Academic Press, 1989:147
7. Lloyd RV, Jin L, Song, J. Ultrastructural localization of prolactin and chromogranin B messenger ribonucleic acids with biotinylated oligonucleotide probes in cultured pituitary cells. Lab Invest 1990;63:413
8. Pomeroy ME, Lawrence JB, Singer RH, Billings–Gagliardi S. Distribution of myosin heavy chain mRNA in embryonic muscle tissue visualized by ultrastructural in situ hybridization. Dev Biol 1991;143:58
9. Childs GV, Yamauchi K, Unabia G. Localization and quantification of hormones, ligands, and mRNA with affinity-gold probes. Am J Anat 1989;185:223
10. Liposits Z, Petersen SL, Paull WK. Amplification of the in situ hybridization signal by postintensification: the biotin-dUTP-streptavidin-peroxidase diaminobenzidine-silver-gold detection system. Histochemistry 1991;96:339
11. Le Guellec D, Trembleau A, Pechoux C, Gossard F, Morel G. Ultrastructural non-radioactive in situ hybridization of GH mRNA in rat pituitary gland: pre-embedding vs ultra-thin frozen sections vs post-embedding. J Histochem Cytochem 1992;40:979
12. Mitchell V, Gambiez A, Beauvillain JC. Fine-structural localization of proenkephalin mRNAs in the hypothalamic magnocellular dorsal nu-

cleus of the guinea pig: a comparison of radioisotopic and enzymatic in situ hybridization methods at the light- and electron microscopic levels. Cell Tissue Res 1993;274:219

13. Deerinck TJ, Martone ME, Lev-Ram V, Green DPL, Tsien RY, Spector DL, Huang S, Ellisman MH. Fluorescence photooxidation with eosin: a method for high resolution immunolocalization and in situ hybridization for light and electron microscopy. J Cell Biol 1994;126:901
14. Sibon OCM, Humbel BM, De Graaf A, Verkleij AJ, Cremers FFM. Ultrastructural localization of epidermal growth factor (EGF)-receptor in the cell nucleus using pre-embedding in situ hybridization in combination with ultra-small gold probes and silver-enhancement. Histochemistry 1994;101:223
15. Huang S, Deerinck TJ, Ellisman MH, Spector DL. In vivo analysis of the stability and transport of nuclear poly(A)$^+$ RNA. J Cell Biol 1994;126:877
16. Wenderoth MP, Eisenberg BR. Ultrastructural distribution of myosin heavy chain mRNA in cardiac tissue: a comparison of frozen and LR White embedment. J Histochem Cytochem 1991;39:1025
17. Dirks RW, Van Dorp AGM, Van Minnen J, Fransen JAM, Van der Ploeg M, Raap AK. Electron microscopic detection of RNA sequences by non-radioactive in situ hybridization in the mollusk *Lymnaea stagnalis*. J Histochem Cytochem 1992;40:1647
18. Matsuno A, Ohsugi Y, Utsunomiya H, Takekoshi S, Osamura RY, Watanabe K, Teramoto A, Kirino T. Ultrastructural distribution of growth hormone and prolactin mRNAs in normal rat pituitary cells: a comparison between preembedding and postembedding methods. Histochemistry 1994;102:265
19. Takizawa T, Robinson JM. Use of 1.4-nm immunogold particles for immunocytochemistry on ultra-thin cryosections. J Histochem Cytochem 1994;42:1615
20. Macville MVE, Van Dorp AGM, Wiesmeijer KC, Dirks RW, Fransen JAM, Raap AK. Monitoring morphology and signal during non-radioactive in situ hybridization procedures by reflection-contrast microscopy and transmission electron microscopy. J Histochem Cytochem 1995;43:665
21. Priestley JV. Pre-embedding ultrastructural immunocytochemistry: immunoenzyme techniques. In Polak JM, Varndell IM, eds. Immunolabeling for electron microscopy. Amsterdam: Elsevier, 1984:37
22. Griffiths G. Fine structure immunocytochemistry. Berlin: Springer-Verlag, 1993
23. Bohn W. A fixation method for improved antibody penetration in electron microscopical immunoperoxidase studies. J Histochem Cytochem 1978;26:293
24. Willingham MC. An alternative fixation-processing method for pre-embedding ultrastructural immunocytochemistry of cytoplasmic antigens: the GBS (glutaraldehyde-borohydride-saponin) procedure. J Histochem Cytochem 1983;31:791
25. Goping G, Yedgar S, Pollard HB, Kuijpers GAJ. Flat embedding and immunolabeling of SW 1116 colon carcinoma cells in LR White: an improved technique in light and electron microscopy. Microsc Res Techn 1992;21:1
26. Yamawaki M, Zurbriggen A, Richard A, Vandevelde M. Saponin treatment for in situ hybridization maintains good morphological preservation. J Histochem Cytochem 1993;41:105
27. Bangham AD, Horne RW. Action of saponin on biological cell membranes. Nature 1962;196:952
28. Seeman P. Transient holes in the erythrocyte membrane during hypotonic hemolysis and stable holes in the membrane after lysis by saponin and lysolecithin. J Cell Biol 1967;32:55
29. Seeman P, Cheng D, Iles GH. Structure of membrane holes in osmotic and saponin hemolysis. J Cell Biol 1973;56:519
30. Ohtsuki I, Manzi RM, Palade GE, Jamieson JD. Entry of macromolecular tracers into cells fixed with low concentrations of aldehyde. Biol Cell 1978;31:119
31. Akiyama T, Takagi S, Sankawa U, Inari S, Saitô H. Saponin-cholesterol interaction in the multibilayers of egg yolk lecithin as studied by deuterium nuclear magnetic resonance: digitonin and its analogues. Biochemistry 1980;19:1904
32. Cornelese-ten Velde I, Wiegant J, Tanke HJ, Ploem JS. Improved detection and quantification of the (immuno)peroxidase product using reflection-contrast microscopy. Histochemistry 1989;92:153
33. Boom R, Geelen JL, Sol CJ, Raap AK, Minnaar RP, Klaver BP, Van der Noordaa J. Establishment of a rat cell line inducible for the expression of human cytomegalovirus immediate early gene products by protein synthesis inhibition. J Virol 1986;58:851
34. Erickson JM, Rushford CL, Dorney DJ, Wilson GN, Schmickel RD. Structure and variation of human ribosomal DNA: molecular analysis of cloned fragments. Gene 1981;16:1
35. Bauman JGJ, Bentvelzen P. Flow cytometric detection of ribosomal RNA in suspended cells by fluorescent in situ hybridization. Cytometry 1988;9:517
36. Brands JHGM, Maassen JA, Van Hemert FJ, Amons R, Möller W. The primary structure of the α subunit of human elongation factor 1. Structural aspects of guanine-nucleotide-binding sites. Eur J Biochem 1986; 155:167
37. Cooke HJ, Hindley J. Cloning of human satellite III DNA: different components are on different chromosomes. Nucleic Acids Res 1979; 6:3177
38. Vreugdenhil E, Jackson JF, Bouwmeester T, Smit AB, Van Minnen J, Van Heerikhuizen H, Klootwijk J, Joosse J. Isolation, characterization and evolutionary aspects of a cDNA clone encoding multiple neuropeptides involved in the stereotyped egg-laying behaviour of the fresh-water snail *Lymnaea stagnalis*. J Neurosci 1988;8:4184
39. Artvinli S. Biochemical aspects of aldehyde fixation and a new formaldehyde fixative. Histochem J 1975;7:435
40. Dirks RW, Van de Rijke FM, Fujishita S, Van der Ploeg M, Raap AK. Methodologies for specific intron and exon RNA localization in cultured cells by haptenized and fluorochromized probes. J Cell Sci 1993;104:1187
41. Raap AK, Van de Rijke FM, Dirks RW, Sol CJ, Boom R, Van der Ploeg M. Bicolor fluorescence in situ hybridization to intron and exon mRNA sequences. Exp Cell Res 1991;197:319
42. Danscher G. Localization of gold in biological tissue. A photochemical method for light and electron microscopy. Histochemistry 1981;71:81
43. Ploem JS. Reflection-contrast microscopy as a tool for investigation of the attachment of living cells to a glass surface. In Van Furth R, ed. Mononuclear phagocytes in immunity, infection and pathology. Oxford: Blackwell, 1975:405
44. Cornelese-Ten Velde I, Bonnet J, Tanke HJ, Ploem JS. Reflection-contrast microscopy. Visualization of (peroxidase-generated) diaminobenzidine polymer products and its underlying optical phenomena. Histochemistry 1988;89:141
45. Thelestam M, Mollby R. Classification of microbial, plant and animal cytolysins based on their membrane-damaging effects on human fibroblasts. Biochim Biophys Acta 1979;557:156
46. Thiry M, Thiry-Blaise L. In situ hybridization at the electron microscope level: an improved method for precise localization of ribosomal DNA and RNA. Eur J Cell Biol 1989;50:235
47. Puvion-Dutilleul F, Bachellerie JP, Puvion E. Nucleolar organization of HeLa cells as studied by in situ hybridization. Chromosoma 1991; 100:395
48. Wachtler F, Mosgoeller W, Schwarzacher HG. Electron microscopic in situ hybridization and autoradiography: localization of transcription of rDNA in human lymphocyte nucleoli. Exp Cell Res 1990;187:346

49. Wachtler F, Stahl A. The nucleolus: a structural and functional interpretation. Micron 1993;24:473

50. Sibon OCM, Cremers FFM, Humbel BM, Boonstra J, Verkleij AJ. Localization of nuclear RNA by pre- and post-embedding in situ hybridization using different gold probes. Histochem J 1995;27:35

51. Dirks RW, Daniel KC, Raap AK. RNAs radiate from gene to cytoplasm as revealed by fluorescence in situ hybridization. J Cell Sci, in press

52. Burry RW, Vandre DD, Hayes DM. Silver-enhancement of gold antibody probes in pre-embedding electron microscopic immunocytochemistry. J Histochem Cytochem 1992;40:1849

53. Gilerovitch HG, Bishop GA, King JS, Burry RW. The use of electron microscopic immunocytochemistry with silver-enhanced 1.4-nm gold particles to localize GAD in the cerebellar nuclei. J Histochem Cytochem 1995;43:337